The Anomalies and Local Structure of Liquid Water from Boiling to the Supercooled Regime as Predicted by the Many-Body MB-pol Model

Thomas E. Gartner III,[†] Kelly M. Hunter,[‡] Eleftherios Lambros,[‡] Alessandro Caruso,[‡] Marc Riera,[‡] Gregory R. Medders,[‡] Athanassios Z. Panagiotopoulos,[¶] Pablo G. Debenedetti,[¶] and Francesco Paesani[*,§,∥,⊥]

†*Department of Chemistry, Princeton University, Princeton, NJ 08544, United States*

‡*Department of Chemistry and Biochemistry, University of California, San Diego, La Jolla, CA 92093, United States*

¶*Department of Chemical and Biological Engineering, Princeton, NJ 08544, United States*

§*Department of Chemistry and Biochemistry, University of California San Diego, La Jolla, California 92093, United States*

∥*Materials Science and Engineering, University of California San Diego, La Jolla, California 92093, United States*

⊥*San Diego Supercomputer Center, University of California San Diego, La Jolla, California 92093, United States*

E-mail: fpaesani@ucsd.edu

Abstract

For the last 50 years, researchers have sought molecular models that can accurately reproduce water's microscopic structure and thermophysical properties across broad ranges of its complex phase diagram. Herein, molecular dynamics simulations with the many-body MB-pol model are performed to monitor the thermodynamic response functions and local structure of liquid water from the boiling point down to deeply supercooled temperatures at ambient pressure. The isothermal compressibility and isobaric heat capacity show maxima near 223 K, in excellent agreement with recent experiments, and the liquid density exhibits a minimum at ∼208 K. A local tetrahedral arrangement, where each water molecule accepts and donates two hydrogen bonds, is found to be the most probable hydrogen-bonding topology at all temperatures. This work suggests that MB-pol may provide predictive capability for studies of liquid water's physical properties across broad ranges of thermodynamic states, including the so-called water's "no man's land" which is difficult to probe experimentally.

Graphical TOC Entry

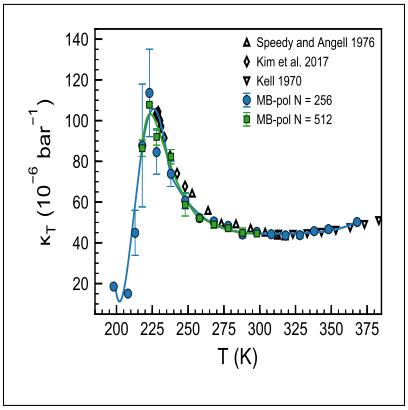

The importance of water cannot be overemphasized, as it is essential for life,[1] being directly involved in several fundamental biological and chemical processes.[2] At ambient pressure, liquid water exhibits anomalous behavior as a function of temperature, which becomes more pronounced at deeply supercooled temperatures.[3] In particular, water's thermodynamic response functions, such as the isothermal compressibility (κ_T),[4] the isobaric heat capacity (c_P),[5] and the thermal expansion coefficient (α_P), appear to diverge as the temperature is decreased towards ∼228 K. Recent ultrafast x-ray measurements have provided evidence that both κ_T[6] and c_P[7] do not actually diverge at ambient pressure, but instead increase sharply below 235 K before reaching their maximum values at 229 K. Other common liquid properties are also distinctive in water: the density (ρ) maximum at 277 K is well known, and the presence of a ρ minimum under deeply supercooled conditions has also been suggested based on experiments on confined water.[8] To a large extent, the unique properties of water can be traced back to the ability of the water molecules to form a dynamic hydrogen-bond network whose structure continually fluctuates in space and time in a temperature-dependent way. However, determining an unambiguous, one-to-one relationship between local structure and thermodynamic response functions in liquid water as the temperature is decreased from the boiling point down to the supercooled regime has so far remained elusive.

The common picture of liquid water at ambient conditions derived from x-ray and neutron scattering experiments[9–12] and NMR measurements[13] assumes that each molecule is, on average, 4-fold coordinated in a tetrahedral environment. This picture was challenged by a new interpretation of x-ray absorption spectra measured for liquid water and ice, suggesting that the coordination number in the liquid phase at ambient conditions is actually closer to two, with each molecule accepting and donating only one hydrogen bond, respectively.[14] Later, x-ray emission spectra of liquid water were found to display two distinct peaks ($1b_1'$ and $1b_1''$) associated with transitions from the non-bonding $1b_1$ to the core $1a_1$ orbitals of the water molecules, while a single peak was observed in analogous spectra measured for crystalline ice.[15] Since the $1b_1'$ and $1b_1''$ peaks in the x-ray emission spectrum of liquid water

were found to vary in intensity as the temperature was decreased from 338.15 K to 280.15 K, the two peaks were interpreted as a manifestation of a bimodal distribution of hydrogen-bonding motifs with an estimated ratio of highly distorted configurations (assigned to the $1b_1''$ peak) to tetrahedral-like configurations (assigned to the $1b_1'$ peak) of 2:1. However, direct experimental observations of such molecular-level details are difficult to obtain, particularly as the temperature is decreased into the supercooled regime. Furthermore, both the observations of a maximum in κ_T[16,17] and a minimum in ρ[18] have been controversial, underscoring the importance of realistic computer simulations that can be used independently to corroborate or challenge the experimental measurements, while providing a direct link between molecular-level structure and thermodynamic response functions. Such computational approaches could also help validate/confirm unifying thermodynamic explanations for water's anomalies, such as the possibility that water exhibits a second critical point in the supercooled liquid.[19–22]

Developing a realistic molecular model of water has been a grand challenge for theoretical/computational chemists and physicists since the first Monte Carlo (MC)[23] and molecular dynamics (MD)[24] simulations of liquid water. Despite remarkable progress in the implementation of efficient quantum mechanical approaches based on either wavefunction theory[25] or density functional theory,[26] and impressive advances in the development of more sophisticated force fields,[27] a molecular model capable of accurately predicting the properties of liquid water from the boiling point down to the supercooled regime is still missing. The last decade has witnessed the emergence of explicit many-body models which, rigorously derived from the many-body expansion of the underlying interaction energies,[28] have shown great promise for predictive simulations of water across the entire phase diagram.[27] Among the existing many-body models, MB-pol[29–32] correctly reproduces structural, thermodynamic, dynamical, and spectroscopic properties of gas-phase water clusters,[33–35] liquid water,[36] the vapor/liquid interface,[37–39] and ice,[40,41] which suggests that MB-pol could provide a reliable link between water's anomalous thermodynamic response functions and molecular-level

structure.

In this study, we perform classical MD simulations with the MB-pol model to monitor the evolution of the thermodynamic response functions and local structure of liquid water, from the boiling point down to deeply supercooled temperatures. Although several MD simulations of supercooled water carried out with various water models have been reported in the literature,[42] none of these simulations have been able to accurately reproduce the experimentally measured variation of κ_T and c_P as the temperature decreases down to $\sim$228 K.[43] Herein, we report the temperature dependence of κ_T, c_P, and ρ obtained from isothermal-isobaric simulations of MB-pol at ambient pressure, as well as the oxygen-oxygen radial distribution function, tetrahedral order parameter, and hydrogen bonding topologies, and compare our simulation results with the latest available experimental data for liquid water across a wide temperature range. Although we performed MD simulations with both $N = 256$ and $N = 512$ molecules, we focus the majority of our discussion on the results for the smaller system since, as shown in Table S1, they were obtained from longer simulations and more temperatures. In this regard it should be noted that the values of κ_T, c_P, and ρ calculated for temperatures above 245 K from shorter MD simulations with with $N = 256$ MB-pol water molecules were reported in Ref. 32.

Fig. 1a shows the variation of the isothermal compressibility at ambient pressure in the temperature range between 198 K and 368 K. In a seminal study, Speedy and Angell[4] extended the original measurements by Kell[44] down to 247 K and observed a power-law increase of κ_T as the temperature was decreased, which is the characteristic behavior of thermodynamic properties in the vicinity of a critical point or a limit of stability. However, using ultrafast x-ray spectroscopy, Kim *et al.*[6] extended the accessible temperature range down to 227 K and detected maxima for both isothermal compressibility and correlation length at 229 K. In the present work, the values of κ_T calculated from MB-pol simulations with 256 water molecules closely follow the experimental data over the entire temperature range. Similar agreement is obtained from analogous simulations with 512 molecules. Impor-

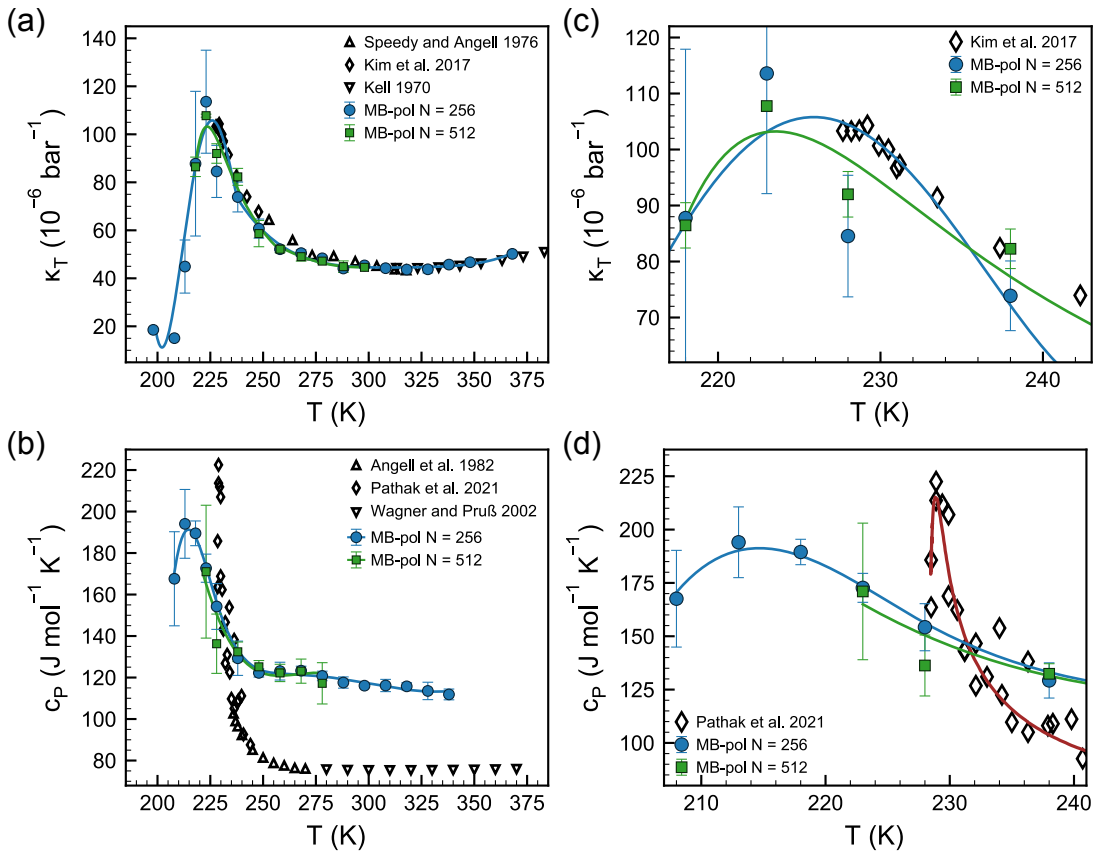

Figure 1: Thermodynamic response functions of liquid water. (a) Isothermal compressibility, κ_T, from experiments in Refs. 4,6,44 (black symbols) and as predicted by MB-pol with N = 256 molecules (blue circles) and N = 512 molecules (green squares). (b) Isobaric heat capacity, c_P, from experiments in Refs. 5,7,45 (black symbols) and as predicted by MB-pol with N = 256 molecules (blue circles) and N = 512 molecules (green squares). (c) and (d) include the same data as (a) and (b), respectively, but with axis scale adjusted to focus on the κ_T and c_P maxima. All solid lines are guides to the eye; solid blue and green lines are polynomial fits to the simulation data, and the red line interpolating the experimental data in (d) is taken from Ref. 7. Error bars in simulation results represent 95% confidence intervals.

tantly, MB-pol with N = 256 predicts a maximum of 113 ± 21×10^{-6} bar^{-1} at 223 K (κ_T = 108 ± 1×10^{-6} bar^{-1} for N = 512), which is in remarkable agreement with the experimental value of ∼105×10^{-6} bar^{-1} (Fig. 1c). Below 223 K, MB-pol predicts a steep decrease of κ_T, which reaches a value of ∼15.1 ± 0.4×10^{-6} bar^{-1} at 208 K. This behavior is consistent with the concept of the Widom line, i.e., a line in the P-T diagram emanating from a critical point at which a thermodynamic response function and associated fluctuations reach maximum

values. It should be noted that the relatively larger error bars associated with the MB-pol results at 218, 223, and 228 K are a direct consequence of the longer relaxation times near the Widom line, as can be seen in the density vs. time results presented in Figs. S1 and S2, and the density autocorrelation functions in Fig. S2d, which indicates relaxation times on the order of several to tens of ns for temperatures below 230 K. We note that while the relaxation time is near to the total simulation length for the lowest temperatures explored, in Fig. S3 we show further evidence for liquid-like structural relaxation at all temperatures studied via the mean-squared displacement and the self-intermediate scattering function of the oxygen atoms. Interestingly, Figs. S2 and S3 may indicate slower liquid-like relaxation at 208 K compared to 198 K, which may correlate with differences in the degree of tetrahedral order between the two state points, as discussed below. However, it is not possible to pinpoint the dynamics quantitatively in these simulations due to the action of the thermostat and barostat. A detailed exploration of the dynamics of MB-pol at deeply supercooled temperatures will be forthcoming; here we merely emphasize the liquid-like nature of the simulations.

To place the MB-pol results in context, it should be noted that popular water models that predict a maximum in κ_T in the range 225-240 K, such as TIP4P/2005 and iAMOEBA, were shown to significantly underestimate (by nearly half) the experimental value, while other models, such as mW and SPC/E, also underestimate the temperature of maximum κ_T by $\sim$20 K.[46] More recently, a neural network potential based on the SCAN density functional was shown to predict a maximum of $\sim 50 \times 10^{-6}$ bar^{-1} at 255 K.[47] One may ask if nuclear quantum effects are the source of part of the discrepancies observed in previous studies, as classical MD simulations neglect the quantum nature of the hydrogen atoms.[48] However, recent path-integral molecular dynamics (PIMD) simulations, which explicitly account for nuclear quantum effects, carried out with the q-TIP4P/F empirical water model show only a moderate increase in the peak value of κ_T relative to the classical MD simulations and no appreciable change in the temperature of maximum κ_T,[49] suggesting that MB-pol's quan-

titative accuracy in reproducing κ_T at ambient pressure should be robust to the choice of treatment of nuclear quantum effects.

The temperature dependence of the heat capacity is shown in Fig. 1b. Also in this case, the MB-pol simulations with $N = 256$ predict a maximum in c_P at 218-223 K, which is close to the temperature (229 K) determined experimentally.[7] The MB-pol results with $N = 512$ are qualitatively similar to $N = 256$ over the explored temperature range, with a sharp increase in c_P as the temperature is decreased. However, due to our approach to calculating the c_P (fitting polynomials to obtain the slope of enthalpy vs. temperature, as described in the supporting information), we can not calculate c_P values for $N = 512$ at temperatures below 223 K. Thus, we report a maximum in c_P only for $N = 256$ due to the longer timescales, better statistics, and wider temperature range accessible for the smaller system. Focusing on the $N = 256$ results, while the qualitative observation of a c_P maximum is preserved, the agreement between measured and calculated c_P values is not quantitative as it is for the κ_T. In particular, the high-temperature values of c_P are larger than the experimental results, and the low-temperature peak in c_P is broader than recent experiments (Fig. 1d). We posit that these differences are due to the c_P being particularly sensitive to nuclear quantum effects relative to other thermodynamic quantities. PIMD simulations with the q-TIP4P/F model have indeed found that the difference between classical and quantum values of c_P is approximately 50 J mol^{-1} K^{-1}.[49] Applying the same difference to the MB-pol results of Fig. 1b would bring the MB-pol values of c_P close to the experimental data above 250 K but, at the same time, would also worsen the agreement with experiment at lower temperature. However, we note that there is no reason to expect that a consistent shift in c_P would be observed across all temperatures,[48] thus necessitating full PIMD simulations with MB-pol at supercooled temperatures to definitively evaluate this discrepancy, which will be the focus of a future study.

The temperature dependence of ρ calculated from MB-pol simulations is shown in Fig. 2 along with the available experimental data; these results show essentially no dependence on

system size. In agreement with previous results, the temperature of maximum density for MB-pol is 263 K, which is 14 K below the experimental value, with an average absolute deviation of 0.013 g cm^{-3} from the experimental data over the temperature range between 247 K and 373 K.[32] At lower temperatures, MB-pol predicts a steep decrease in ρ from 250 K down to 208 K, where ρ reaches a minimum of 0.91 g cm^{-3} before increasing again at 198 K. The temperature of minimum density near 208 K is in very close agreement with the ∼210 K density minimum observed for heavy water confined in nanopores,[8] as shown in Fig. S4. It should be noted that a ρ minimum was found in bulk NPT simulations with several empirical water models, including TIP4P/2005,[51] TIP5P-E,[52] and others.[53,54] Thus, the fact that this phenomenon is also observed in the many-body MB-pol model serves as additional corroboration that a minimum in ρ is possible in real bulk water.

The ability of MB-pol to reproduce, with quantitative accuracy, the experimentally observed maxima in κ_T and c_P upon supercooling, and its realistic (if not fully quantitatively accurate) representation of the density anomaly, suggest that MB-pol indeed provides a realistic representation of liquid water along the 1 atm isobar. Therefore, analysis of the NPT trajectories obtained with the MB-pol model should provide an accurate window into the evolution of the structure of liquid water from the boiling point down to deeply supercooled

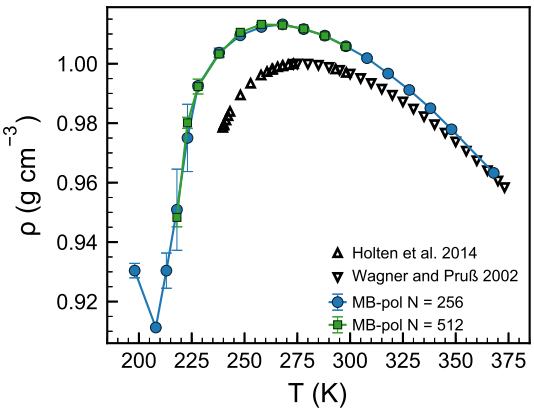

Figure 2: Mass density of liquid water. Density, ρ, from experiments in Refs. 45,50 (black symbols) and as predicted by MB-pol with $N = 256$ (blue circles) and $N = 512$ (green squares). Error bars in simulation results represent 95% confidence intervals.

temperatures. In this context, the oxygen-oxygen (g_{OO}) radial distribution function (RDF) shown in Fig. 3a as a function of temperature displays the expected trend, with g_{OO} becoming progressively more structured as the temperature decreases. Fig. S5 shows that MB-pol is in quantitative agreement with the most recent experimental RDFs derived from x-ray diffraction measurements.[12,55] The evolution of g_{OO} upon cooling is directly mirrored by a progressive variation in the underlying 3-dimensional hydrogen-bond network, as characterized by probability distributions of the tetrahedral order parameter, $P(q_{tet})$, shown in Fig. 3b. The definition of q_{tet}, as well as movies showing the instantaneous value of q_{tet} associated with each water molecule along the MD trajectories at different temperatures, are available in the Supporting Information. A value of 1 for q_{tet} corresponds to perfectly tetrahedral arrangements of the water molecules, while $q_{tet} = 0$ corresponds to completely disordered arrangements (as in an ideal gas). At the higher temperatures, $P(q_{tet})$ extends over the entire range of q_{tet}, with a small peak at $q_{tet} \approx 0.5$. At intermediate temperatures $P(q_{tet})$ is bimodal, with the second peak at $q_{tet} \approx 0.8$ progressively growing in intensity and shifting to higher q_{tet} values as the temperature decreases. This trend is accompanied by the progressive disappearance of the peak initially located at $q_{tet} \approx 0.5$. Fig. S6 shows that molecules with high or low values of q_{tet} are uniformly distributed throughout the fluid at all temperatures. Although the temperature ranges were different, qualitatively similar trends for both g_{OO}[56] and $P(q_{tet})$[42] were observed in simulations with various empirical water models.

To provide further insights into the evolution of the water structure upon cooling, the temperature dependence of the hydrogen-bond network is analyzed in terms of each contributing hydrogen-bonding topology. It should be noted that analyses using different structural descriptors have recently been reported for MD simulations of supercooled water carried out with models which, however, fail to correctly reproduce both the location and magnitude of the experimental maxima of the thermodynamic response functions.[57–59]

In the present analysis, the hydrogen-bonding topologies are determined by using a geo-

metric definition of hydrogen bonds, and each water molecule is classified according to the number of donor (D) and acceptor (A) hydrogen bonds in which it participates. Fig. 3c shows that the fully tetrahedral topology, where a water molecule simultaneously accepts and donates two hydrogen bonds (2_D2_A), is the most common hydrogen-bonding arrangement at all temperatures. The probability of finding 2_D2_A molecules is ∼30% at 368 K and monotonically increases as the temperature decreases, displaying a steeper increase between 238 K and 220 K before saturating to >90% below 220 K. An analogous rapid increase of tetrahedral structures at deeply supercooled temperatures was recently observed experimentally,[6] and the predominance of the 2_D2_A topology at low temperatures was also noted in the TIP4P/Ice empirical water model.[60] In the present MB-pol results, water molecules that donate two hydrogen bonds but only accept one hydrogen bond constitute the second most probable topology over the entire temperature range, representing ∼20-25% of all possible hydrogen-bonding topologies between 368 K and 278 K before quickly disappearing at lower temperatures. Similar temperature dependence is displayed by the 1_D2_A topology. The only other contributing hydrogen-bonding topology is the 1_D1_A topology, where a water molecule only donates and accepts a single hydrogen bond. The probability of the 1_D1_A topology

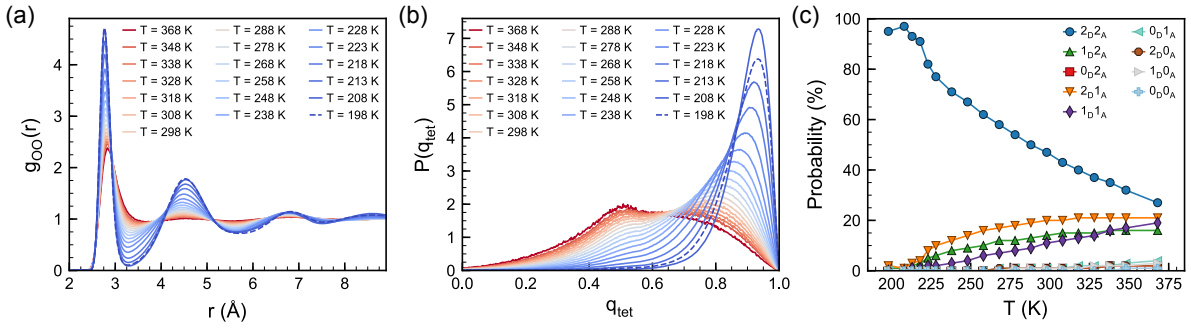

Figure 3: Local structure of liquid water. (a) Oxygen-oxygen radial distribution function, g_{OO}, (b) probability distribution of the tetrahedral order parameter, $P(q_{tet})$, and (c) probability of hydrogen bonding topologies as a function of temperature. In (a) and (b), colors denote different temperatures as marked, and in (c), colors and symbols denote different hydrogen-bonding arrangements as marked. $T = 198$ K data in (a) and (b) are plotted in dashed lines to emphasize the difference between the $T = 208$ K and $T = 198$ K results. All data in this figure are with $N = 256$ molecules.

decreases linearly with temperature, being ∼20% at 368 K and less than 5% below 270 K. Importantly, the MB-pol simulations carried out at 298 K predict that the probability of the 1_D1_A topology is ∼10%, which is in stark contrast with the estimate of 80%±20% derived from the analysis of the experimental x-ray absorption spectra.[14] Given the agreement provided by MB-pol with experimental data for κ_T, c_P, and ρ upon cooling (Figs. 1-2), as well as for several other properties of water across broad regions of its phase diagram,[32] the proposal of liquid water being primarily composed of water molecules with one strong donor and one strong acceptor[14] appears to be unsupported by the present results. In turn, the absence of a predominant fraction of 1_D1_A molecules at ambient temperature also challenges the interpretation that the temperature dependence of the x-ray emission spectrum of liquid water in the $1b_1$ region can be explained by a structural transformation of 1_D1_A molecules into 2_D2_A molecules as the temperature decreases. By contrast, these MB-pol results provide support to a recent theoretical analysis of the x-ray emission spectrum of liquid water showing that the observed $1b_1$ splitting cannot be attributed to any specific hydrogen-bonding topology.[61]

Importantly, we note that the structural results presented in Fig. 3 provide a possible explanation for the anomalous slower structural relaxation we observed at 208 K compared to 198 K (Figs. S2 and S3). Fig. 3b shows that the distribution of q_{tet} values is narrower for 208 K, with a higher peak value of $P(q_{tet})$ compared to 198 K. In parallel, the 2_D2_A hydrogen-bonding topology is more prevalent at 208 K compared to 198 K (Fig. 3c). These trends indicate a more perfectly tetrahedral local structure at 208 K, which correlates with the minimum in density and also likely explains the anomalous maximum in the timescale of structural relaxation at that temperature. As mentioned above, our observation of anomalous relaxation dynamics near the density minimum necessitates further study, due to the influence of the thermostat and barostat on the simulations performed in this present work.

In summary, we used MD simulations with the many-body MB-pol model to monitor the evolution of several thermodynamic response functions of liquid water, from the boil-

ing point down to deeply supercooled temperatures. The agreement provided by MB-pol with key aspects of experimental data for the isothermal compressibility, heat capacity, and liquid density over the entire temperature range lends credence to the underlying molecular-level picture of liquid water, which progressively and continuously transforms from a system containing several hydrogen-bonding topologies at high temperature to a nearly perfect tetrahedral liquid below 230 K. MB-pol also predicts maxima in the isothermal compressibility and heat capacity near 223 K, which provides support to recent experimental measurements that located the maxima in both thermodynamic response functions at ∼229 K. Our results also help corroborate the experimental observation of a density minimum in confined water, and suggest that such a phenomenon may also exist in bulk supercooled liquid water.

While the present results are limited to common structural and thermodynamic properties at ambient pressure, future work could include evaluating whether MB-pol is consistent with recent experimental and simulation work that interpret ambient-pressure liquid water as containing two types of interconvertible local structural motifs.[62,63] Further, MB-pol could be used to explore water's metastable phase behavior in detail, including evaluating the possibility of a liquid-liquid critical point at elevated pressures. However, we note that given MB-pol's higher computational cost relative to empirical pairwise additive models,[32] such an effort would likely necessitate combining ongoing work to implement MB-pol in highly-parallelizable and optimized simulation software[39] with the use of enhanced sampling methods[47] to properly account for sluggish structural relaxation in the deeply supercooled liquid. Such optimized codes and advanced approaches may in the future enable the study of larger system sizes and/or full PIMD simulations to help definitively link water's phase behavior and thermodynamic properties with its local structure(s). The present calculations show that the MB-pol model is able to capture significant aspects of liquid water's behavior over a range of temperatures from the boiling point to deeply supercooled conditions at atmospheric pressure. In particular, the model reproduces, with quantitative accuracy, the experimentally observed maxima in compressibility and heat capacity upon supercooling.

While the model's behavior at different pressures remains to be explored, the results reported herein suggest that MB-pol may open the door to quantitatively reliable studies of water's thermophysical properties and their underlying molecular basis.

Supporting Information Available

Details about the MD simulations. Additional table with details about the length of the MD simulations carried out at different temperatures. Additional figures showing the density fluctuations and the density time correlation functions at different temperatures, dynamics of structural relaxation at low temperatures, a comparison with the experimental density of heavy water in confinement, the experimental and simulated oxygen-oxygen radial distribution functions at different temperatures, and the spatial distributions of the tetrahedral order parameter at different temperatures. All data generated and analyzed in this study which are not reported in the Supporting Information are available from the authors upon request.

Acknowledgement

We thank the late Prof. Austen Angell for countless, stimulating conversations about the properties of supercooled water and his continued support to the development of the MB-pol water model. This research was supported by the Air Force Office of Scientific Research under award no. FA9550-20-1-0351 (F.P.), the "Chemistry in Solution and at Interfaces" (CSI) Center that is funded by the U.S. Department of Energy under award no. DE-SC001934 (A.Z.P. and P.G.D.), and the National Science Foundation under award no. CHE-1856704 (P.G.D.). Computational resources were provided by the Department of Defense High Performance Computing Modernization Program (HPCMP), the Triton Shared Computing Cluster (TSCC) at the San Diego Supercomputer Center (SDSC) Supercomputer Center (SDSC), and Princeton Research Computing, a consortium of groups including the Princeton Institute

for Computational Science and Engineering (PICSciE) and the Office of Information Technology's High Performance Computing Center and Visualization Laboratory at Princeton University.

References

(1) Franks, F. *Water: A Matrix of Life*; Royal Society of Chemistry, 2000; Vol. 21.

(2) Bagchi, B. *Water in Biological and Chemical Processes: From Structure and Dynamics to Function*; Cambridge University Press, 2013.

(3) Debenedetti, P. G. Supercooled and Glassy Water. *J. Condens. Matter Phys.* **2003**, *15*, R1669.

(4) Speedy, R.; Angell, C. Isothermal Compressibility of Supercooled Water and Evidence for a Thermodynamic Singularity at -45 ^{o}C. *J. Chem. Phys.* **1976**, *65*, 851–858.

(5) Angell, C.; Sichina, W.; Oguni, M. Heat Capacity of Water at Extremes of Supercooling and Superheating. *J. Phys. Chem.* **1982**, *86*, 998–1002.

(6) Kim, K. H.; Späh, A.; Pathak, H.; Perakis, F.; Mariedahl, D.; Amann-Winkel, K.; Sellberg, J. A.; Lee, J. H.; Kim, S.; Park, J., et al. Maxima in the Thermodynamic Response and Correlation Functions of Deeply Supercooled Water. *Science* **2017**, *358*, 1589–1593.

(7) Pathak, H.; Späh, A.; Esmaeildoost, N.; Sellberg, J. A.; Kim, K. H.; Perakis, F.; Amann-Winkel, K.; Ladd-Parada, M.; Koliyadu, J.; Lane, T. J., et al. Enhancement and Maximum in the Isobaric Specific-Heat Capacity Measurements of Deeply Supercooled Water Using Ultrafast Calorimetry. *Proc. Natl. Acad. Sci. U.S.A.* **2021**, *118*, e2018379118.

(8) Liu, D.; Zhang, Y.; Chen, C.-C.; Mou, C.-Y.; Poole, P. H.; Chen, S.-H. Observation of the Density Minimum in Deeply Supercooled Confined Water. *Proc. Natl. Acad. Sci. U.S.A.* **2007**, *104*, 9570–9574.

(9) Sorenson, J. M.; Hura, G.; Glaeser, R. M.; Head-Gordon, T. What Can X-ray Scattering Tell Us About the Radial Distribution Functions of Water? *J. Chem. Phys.* **2000**, *113*, 9149–9161.

(10) Soper, A. The Radial Distribution Functions of Water and Ice from 220 to 673 K and at Pressures up to 400 MPa. *Chem. Phys.* **2000**, *258*, 121–137.

(11) Soper, A.; Benmore, C. Quantum Differences Between Heavy and Light Water. *Phys. Rev. Lett.* **2008**, *101*, 065502.

(12) Skinner, L. B.; Huang, C.; Schlesinger, D.; Pettersson, L. G.; Nilsson, A.; Benmore, C. J. Benchmark Oxygen-Oxygen Pair-Distribution Function of Ambient Water from X-ray Diffraction Measurements with a Wide Q-Range. *J. Chem. Phys.* **2013**, *138*, 074506.

(13) Modig, K.; Pfrommer, B. G.; Halle, B. Temperature-Dependent Hydrogen-Bond Geometry in Liquid Water. *Phys. Rev. Lett.* **2003**, *90*, 075502.

(14) Wernet, P.; Nordlund, D.; Bergmann, U.; Cavalleri, M.; Odelius, M.; Ogasawara, H.; Näslund, L.-Å.; Hirsch, T.; Ojamäe, L.; Glatzel, P.; Pettersson, L. G. M.; Nilsson, A. The Structure of the First Coordination Shell in Liquid Water. *Science* **2004**, *304*, 995–999.

(15) Tokushima, T.; Harada, Y.; Takahashi, O.; Senba, Y.; Ohashi, H.; Pettersson, L. G.; Nilsson, A.; Shin, S. High Resolution X-ray Emission Spectroscopy of Liquid Water: The Observation of Two Structural Motifs. *Chem. Phys. Lett.* **2008**, *460*, 387–400.

(16) Caupin, F.; Holten, V.; Qiu, C.; Guillerm, E.; Wilke, M.; Frenz, M.; Teixeira, J.;

Soper, A. K. Comment on "Maxima in the Thermodynamic Response and Correlation Functions of Deeply Supercooled Water". *Science* **2018**, *360*, eaat1634.

(17) Kim, K. H.; Späh, A.; Pathak, H.; Perakis, F.; Mariedahl, D.; Amann-Winkel, K.; Sellberg, J. A.; Lee, J. H.; Kim, S.; Park, J.; Nam, K. H.; Katayama, T.; Nilsson, A. Response to Comment on "Maxima in the Thermodynamic Response and Correlation Functions of Deeply Supercooled Water". *Science* **2018**, *360*, eaat1729.

(18) Soper, A. K. Density Minimum in Supercooled Confined Water. *Proc. Natl. Acad. Sci. U.S.A.* **2011**, *108*, E1192–E1192.

(19) Poole, P. H.; Sciortino, F.; Essmann, U.; Stanley, H. E. Phase Behaviour of Metastable Water. *Nature* **1992**, *360*, 324–328.

(20) Palmer, J. C.; Poole, P. H.; Sciortino, F.; Debenedetti, P. G. Advances in Computational Studies of the Liquid–Liquid Transition in Water and Water-Like Models. *Chem. Rev.* **2018**, *118*, 9129–9151.

(21) Palmer, J. C.; Martelli, F.; Liu, Y.; Car, R.; Panagiotopoulos, A. Z.; Debenedetti, P. G. Metastable Liquid-Liquid Transition in a Molecular Model of Water. *Nature* **2014**, *510*, 385–388.

(22) Debenedetti, P. G.; Sciortino, F.; Zerze, G. H. Second Critical Point in Two Realistic Models of Water. *Science* **2020**, *369*, 289–292.

(23) Barker, J.; Watts, R. Structure of Water; A Monte Carlo Calculation. *Chem. Phys. Lett.* **1969**, *3*, 144–145.

(24) Rahman, A.; Stillinger, F. H. Molecular Dynamics Study of Liquid Water. *J. Chem. Phys.* **1971**, *55*, 3336–3359.

(25) Del Ben, M.; Schönherr, M.; Hutter, J.; VandeVondele, J. Bulk Liquid Water at Ambient Temperature and Pressure from MP2 Theory. *J. Phys. Chem. Lett.* **2013**, *4*, 3753–3759.

(26) Gillan, M. J.; Alfè, D.; Michaelides, A. Perspective: How Good Is DFT for Water? *J. Chem. Phys.* **2016**, *144*, 130901.

(27) Cisneros, G. A.; Wikfeldt, K. T.; Ojamäe, L.; Lu, J.; Xu, Y.; Torabifard, H.; Bartók, A. P.; Csányi, G.; Molinero, V.; Paesani, F. Modeling Molecular Interactions in Water: From Pairwise to Many-Body Potential Energy Functions. *Chem. Rev.* **2016**, *116*, 7501–7528.

(28) Hankins, D.; Moskowitz, J.; Stillinger, F. Water Molecule Interactions. *J. Chem. Phys.* **1970**, *53*, 4544–4554.

(29) Babin, V.; Leforestier, C.; Paesani, F. Development of a "First Principles" Water Potential With Flexible Monomers: Dimer Potential Energy Surface, VRT Spectrum, and Second Virial Coefficient. *J. Chem. Theory Comput.* **2013**, *9*, 5395–5403.

(30) Babin, V.; Medders, G. R.; Paesani, F. Development of a "First Principles" Water Potential With Flexible Monomers. II: Trimer Potential Energy Surface, Third Virial Coefficient, and Small Clusters. *J. Chem. Theory Comput.* **2014**, *10*, 1599–1607.

(31) Medders, G. R.; Babin, V.; Paesani, F. Development of a "First Principles" Water Potential With Flexible Monomers. III. Liquid Phase Properties. *J. Chem. Theory Comput.* **2014**, *10*, 2906–2910.

(32) Reddy, S. K.; Straight, S. C.; Bajaj, P.; Huy Pham, C.; Riera, M.; Moberg, D. R.; Morales, M. A.; Knight, C.; Götz, A. W.; Paesani, F. On the Accuracy of the MB-pol Many-Body Potential for Water: Interaction Energies, Vibrational Frequencies, and Classical Thermodynamic and Dynamical Properties from Clusters to Liquid Water and Ice. *J. Chem. Phys.* **2016**, *145*, 194504.

(33) Richardson, J. O.; Pérez, C.; Lobsiger, S.; Reid, A. A.; Temelso, B.; Shields, G. C.; Kisiel, Z.; Wales, D. J.; Pate, B. H.; Althorpe, S. C. Concerted Hydrogen-Bond Breaking by Quantum Tunneling in the Water Hexamer Prism. *Science* **2016**, *351*, 1310–1313.

(34) Cole, W. T.; Farrell, J. D.; Wales, D. J.; Saykally, R. J. Structure and Torsional Dynamics of the Water Octamer from THz Laser Spectroscopy Near 215 μm. *Science* **2016**, *352*, 1194–1197.

(35) Brown, S. E.; Götz, A. W.; Cheng, X.; Steele, R. P.; Mandelshtam, V. A.; Paesani, F. Monitoring Water Clusters "melt" Through Vibrational Spectroscopy. *J. Am. Chem. Soc.* **2017**, *139*, 7082–7088.

(36) Reddy, S. K.; Moberg, D. R.; Straight, S. C.; Paesani, F. Temperature-Dependent Vibrational Spectra and Structure of Liquid Water from Classical and Quantum Simulations with the MB-pol Potential Energy Function. *J. Chem. Phys.* **2017**, *147*, 244504.

(37) Medders, G. R.; Paesani, F. Dissecting the Molecular Structure of the Air/Water Interface from Quantum Simulations of the Sum-Frequency Generation Spectrum. *J. Am. Chem. Soc.* **2016**, *138*, 3912–3919.

(38) Moberg, D. R.; Straight, S. C.; Paesani, F. Temperature Dependence of the Air/Water Interface Revealed by Polarization Sensitive Sum-Frequency Generation Spectroscopy. *J. Phys. Chem. B* **2018**, *122*, 4356–4365.

(39) Muniz, M. C.; Gartner, T. E.; Riera, M.; Knight, C.; Yue, S.; Paesani, F.; Panagiotopoulos, A. Z. Vapor–Liquid Equilibrium of Water with the MB-pol Many-Body Potential. *J. Chem. Phys.* **2021**, *154*, 211103.

(40) Pham, C. H.; Reddy, S. K.; Chen, K.; Knight, C.; Paesani, F. Many-Body Interactions in Ice. *J. Chem. Theory Comput.* **2017**, *13*, 1778–1784.

(41) Moberg, D. R.; Straight, S. C.; Knight, C.; Paesani, F. Molecular Origin of the Vibrational Structure of Ice I_h. *J. Phys. Chem. Lett.* **2017**, *8*, 2579–2583.

(42) Gallo, P.; Amann-Winkel, K.; Angell, C. A.; Anisimov, M. A.; Caupin, F.; Chakravarty, C.; Lascaris, E.; Loerting, T.; Panagiotopoulos, A. Z.; Russo, J.; Sellberg, J. A.; Stanley, H. E.; Tanaka, H.; Vega, C.; Xu, L.; Pettersson, L. G. M. Water: A Tale of Two Liquids. *Chem. Rev.* **2016**, *116*, 7463–7500.

(43) Späh, A.; Pathak, H.; Kim, K. H.; Perakis, F.; Mariedahl, D.; Amann-Winkel, K.; Sellberg, J. A.; Lee, J. H.; Kim, S.; Park, J., et al. Apparent Power-Law Behavior of Water's Isothermal Compressibility and Correlation Length Upon Supercooling. *Phys. Chem. Chem. Phys.* **2019**, *21*, 26–31.

(44) Kell, G. S. Isothermal Compressibility of Liquid Water at 1 atm. *J. Chem. Eng. Data* **1970**, *15*, 119–122.

(45) Wagner, W.; Pruß, A. The IAPWS Formulation 1995 for the Thermodynamic Properties of Ordinary Water Substance for General and Scientific Use. *J. Phys. Chem. Ref. Data* **2002**, *31*, 387–535.

(46) Pathak, H.; Palmer, J.; Schlesinger, D.; Wikfeldt, K. T.; Sellberg, J. A.; Pettersson, L. G.; Nilsson, A. The Structural Validity of Various Thermodynamical Models of Supercooled Water. *J. Chem. Phys.* **2016**, *145*, 134507.

(47) Gartner, T. E.; Zhang, L.; Piaggi, P. M.; Car, R.; Panagiotopoulos, A. Z.; Debenedetti, P. G. Signatures of a Liquid–Liquid Transition in an Ab Initio Deep Neural Network Model for Water. *Proc. Natl. Acad. Sci. U.S.A.* **2020**, *117*, 26040–26046.

(48) Ceriotti, M.; Fang, W.; Kusalik, P. G.; McKenzie, R. H.; Michaelides, A.; Morales, M. A.; Markland, T. E. Nuclear Quantum Effects in Water and Aqueous Systems: Experiment, Theory, and Current Challenges. *Chem. Rev.* **2016**, *116*, 7529–7550.

(49) Eltareb, A.; Lopez, G. E.; Giovambattista, N. Nuclear Quantum Effects on the Thermodynamic, Structural, and Dynamical Properties of Water. *Phys. Chem. Chem. Phys.* **2021**, *23*, 6914–6928.

(50) Holten, V.; Sengers, J. V.; Anisimov, M. A. Equation of State for Supercooled Water at Pressures up to 400 MPa. *J. Phys. Chem. Ref. Data* **2014**, *43*, 043101.

(51) Russo, J.; Tanaka, H. Understanding Water's Anomalies with Locally Favoured Structures. *Nat. Commun.* **2014**, *5*, 1–11.

(52) Paschek, D. How the Liquid-Liquid Transition Affects Hydrophobic Hydration in Deeply Supercooled Water. *Phys. Rev. Lett.* **2005**, *94*, 217802.

(53) Poole, P. H.; Saika-Voivod, I.; Sciortino, F. Density Minimum and Liquid–Liquid Phase Transition. *J. Phys.: Condens. Matter* **2005**, *17*, L431–L437.

(54) Li, Y.; Li, J.; Wang, F. Liquid–Liquid Transition in Supercooled Water Suggested by Microsecond Simulations. *Proc. Natl. Acad. Sci. U.S.A.* **2013**, *110*, 12209–12212.

(55) Skinner, L. B.; Benmore, C.; Neuefeind, J. C.; Parise, J. B. The Structure of Water Around the Compressibility Minimum. *J. Chem. Phys.* **2014**, *141*, 214507.

(56) Camisasca, G.; Pathak, H.; Wikfeldt, K. T.; Pettersson, L. G. Radial Distribution Functions of Water: Models vs Experiments. *J. Chem. Phys.* **2019**, *151*, 044502.

(57) Martelli, F. Unravelling the Contribution of Local Structures to the Anomalies of Water: The Synergistic Action of Several Factors. *J. Chem. Phys.* **2019**, *150*, 094506.

(58) Formanek, M.; Martelli, F. Probing the Network Topology in Network-Forming Materials: The Case of Water. *AIP Adv.* **2020**, *10*, 055205.

(59) Martelli, F. Topology and Complexity of the Hydrogen Bond Network in Classical Models of Water. *J. Mol. Liq.* **2021**, *329*, 115530.

(60) Foffi, R.; Russo, J.; Sciortino, F. Structural and Topological Changes Across the Liquid–Liquid Transition in Water. *J. Chem. Phys.* **2021**, *154*, 184506.

(61) Cruzeiro, V. W. D.; Wildman, A.; Li, X.; Paesani, F. Relationship Between Hydrogen-Bonding Motifs and the $1b_1$ Splitting in the X-ray Emission Spectrum of Liquid Water. *J. Phys. Chem. Lett.* **2021**, *12*, 3996–4002.

(62) Kringle, L.; Thornley, W. A.; Kay, B. D.; Kimmel, G. A. Reversible Structural Transformations in Supercooled Liquid Water from 135 to 245 K. *Science* **2020**, *369*, 1490–1492.

(63) Shi, R.; Tanaka, H. Direct Evidence in the Scattering Function for the Coexistence of Two Types of Local Structures in Liquid Water. *J. Am. Chem. Soc.* **2020**, *142*, 2868–2875.